Anisotropic Electric Conductivity of Delafossite $PdCoO_2$ Studied by Angle-Resolved Photoemission Spectroscopy

Han-Jin Noh,[1,*] Jinwon Jeong,[1] Jinhwan Jeong,[1] En-Jin Cho,[1] Sung Baek Kim,[2] Kyoo Kim,[3] B. I. Min,[3] and Hyeong-Do Kim[4,†]

[1]*Department of Physics, Chonnam National University, Gwangju 500-757, Korea*
[2]*Laboratory of Pohang Emergent Materials and Department of Physics, POSTECH, Pohang 790-784, Korea*
[3]*Department of Physics, Pohang University of Science and Technology, Pohang 790-784, Korea*
[4]*Pohang Accelerator Laboratory, Pohang University of Science and Technology, Pohang 790-784, Korea*

(Received 11 March 2009; published 24 June 2009)

An explicit connection between the electronic structure and the anisotropic high conductivity of delafossite-type $PdCoO_2$ has been established by angle-resolved photoemission spectroscopy (ARPES) and core-level x-ray photoemission spectroscopy. The ARPES spectra show that a large hexagonal electronlike Fermi surface (FS) consists of very dispersive Pd 4*d* states. The carrier velocity and lifetime are determined from the ARPES data, and the conductivity is calculated by a solution of the Boltzmann equation, which demonstrates that the high anisotropic conductivity originates from the high carrier velocity, the large two-dimensional FS, and the long lifetime of the carriers.

DOI: 10.1103/PhysRevLett.102.256404 PACS numbers: 71.20.−b, 71.15.Mb, 72.80.Ga, 79.60.Bm

Low dimensionality is one of the most fundamental frameworks that make numerous intriguing physical phenomena in solids. High-temperature superconductivity in layered cuprates [1], charge density wave in quasi-two-dimensional transition-metal dichalcogenides [2], and Dirac Fermions in graphene [3] are exemplified for this statement. Delafossite-type $PdCoO_2$ is another example that shows a peculiar property with the two-dimensional structure [4]. While most of the delafossite-type materials are antiferromagnetic insulators, some of them are famous for the transparent conducting property with *p*- or *n*-type carriers such as $CuAlO_2$ and $AgInO_2$, which show relatively good conductivity in the in-plane direction in contrast to poor conductivity along the normal direction [5,6]. The anisotropy of the conductivity, which basically arises from the quasi-two-dimensional nature of the compounds, becomes more intense in $PdCoO_2$ and $PtCoO_2$.

More interesting feature in $PdCoO_2$ and $PtCoO_2$ is the value itself of the conductivity. Previous transport measurement has reported that the in-plane resistivity of $PdCoO_2$ at 260 K is 4.689 $\mu\Omega$cm [7]. This is the lowest value ever reported in the normal state oxides, and even lower than that of Pd metal, 11 $\mu\Omega$cm [8]. Naturally, the succedent studies have focused on the origin of the good conductivity [9,10]. Tanaka *et al.* have given the *s-d* hybridization model of the monovalent Pd ions and coordinated oxygens for the good in-plane conductivity, based on the photon energy dependent photoemission study which indicates that Pd 4*d* mainly contributes to the density of states (DOS) at the Fermi level [9]. The model is reasonable only when the monovalent Pd ions form metallic layers. However, neither the monovalency nor the metallicity of the Pd layer only has been directly confirmed by photoemission spectroscopy, while the Co ions were checked to be trivalent by x-ray absorption [9].

To find the origin of the good in-plane conductivity, an explicit conductivity derivation from the measured electronic structure of $PdCoO_2$ can be an appropriate approach. Several theoretical studies on the band structure of $PdCoO_2$ have been reported [11–13]. In particular, Eyert *et al.* have focused on the orbital character of the conduction band, and have given a conclusion that the electric conductivity is maintained almost exclusively by the Pd 4*d* states [13]. But, to our knowledge, the band structure has not yet been experimentally confirmed. Thus, angle-resolved photoemission spectroscopy (ARPES) could be the most suitable technique to resolve the suspending issues about $PdCoO_2$, because all information required for the conductivity derivation can be obtained from the ARPES data. In this Letter, we present high-resolution core-level x-ray photoemission spectroscopy (XPS) and ARPES spectra of $PdCoO_2$ in order to investigate the origin of its anisotropic high conductivity. Our XPS spectra provide some physical implications for the directional anisotropy of the conductivity in $PdCoO_2$. In addition, an explicit connection between the conductivity and the electronic band structure measured by ARPES is established, showing that the high in-plane conductivity originates from three factors: the *sp* bandlike fast dispersion of a Pd 4*d* conduction band, a large two-dimensional Fermi surface (FS), and the long lifetimes of conducting carriers.

The single crystals of $PdCoO_2$ were grown by the metathetical reaction method as described in the literature [7]. The obtained crystals are silvery hexagonal plates, and the typical size is $2 \times 2 \times 0.1$ mm^3. The single phase was checked by x-ray diffraction. The photoemission experiments were performed at the 3A1 beamline of the Pohang

Light Source with a Scienta SES-2002 electron spectrometer [14]. The photon energy was set to $\hbar\omega = 120$ eV (1000 eV) for ARPES (XPS), and the total energy resolution is ~60 meV (0.8 eV). The momentum resolution was set to be ~0.01 $Å^{-1}$. The crystals were cleaved *in situ* by the top post method at the temperature of 20 K under the pressure of $\sim 7.0 \times 10^{-11}$ Torr. Because of the two-dimensional structure of the crystals, the cleaved surface was shiny and well oriented. During the measurements, the sample temperature was kept to 20 K.

The crystal structure of $PdCoO_2$ ($R\bar{3}m$) is shown in Fig. 1(a) and the corresponding Brillouin zone (BZ) in Fig. 1(b). The structure has two kinds of layers. One is a triangular PdO_2 layer and the other is a triangular CoO_2 layer. These layers are stacked up alternately, sharing all the oxygen ions. In the CoO_2 layer, a Co ion sits in the center of an oxygen octahedron. Trigonally distorted CoO_6 octahedron shares its edges with the nearest CoO_6's, forming a triangular lattice. This stack view to the lattice structure, which is eventually related to the two dimensionality of the system, helps us to understand the basic electronic structure of $PdCoO_2$. The Co ions are trivalent with a low-spin configuration. This was confirmed by our Co $2p$ x-ray absorption spectrum which shows a much more clear sign of Co^{3+} ion than previous one [9]. If six electrons in the Co^{3+} ion fully occupy the triply degenerate t_{2g} orbitals, the spin quantum number is $S = 0$. This explains the small value of the magnetic susceptibility in the previous studies [7]. The Pd ions are inferred to be monovalent, so one d hole resides in a Pd ion in a simple ionic picture. If we regard the system as two separate layers and consider the valence states of the ions, the PdO_2 layer should be a metal and the CoO_2 layer an insulator.

Interestingly, contrasting spectroscopic evidence supporting this simple metal-insulator stack picture is found as shown in Fig. 2. The Pd $3d$ XPS spectrum of $PdCoO_2$ in Fig. 2(a) looks like a metallic core-level photoelectron spectrum, i.e., asymmetric line shape and small plasmonic energy loss structures (▽) typically observed in a good metallic sample. A core hole produced by photoemission process attracts conduction electrons to excite many electron-hole pairs across the Fermi level, resulting in an asymmetric line shape. This is well described by the Mahan, Nozières, and De Dominicis model [15,16], with which the core-level line shape was calculated by Doniach and Šunjić (DS) [17]. To be more quantitative, we fitted the DS line shape function (red line) for our experimental spectrum (black dots) and obtained the asymmetric parameter of $\alpha = 0.26$. This value is a little larger than that for Pd metal, but resides in a reasonable region [18,19]. Contrary to the Pd case, Co $2p$ XPS spectrum presented in Fig. 2(b) shows typical features of correlated insulators. The prominent satellite structure is far from a good metallic behavior. The satellite peaks are well explained by the charge transferred states in the configuration-interaction cluster model [20,21]. The blue bars and a red line in Fig. 2(b) are the relative transition amplitudes of the photoemission process and a broadened spectrum from the transition probabilities based on the model calculation, respectively. Assuming that the ground state of the CoO_6 cluster is a d^6 low-spin ($^1A_1$, $S = 0$) state, the Co $2p$ spectrum is fitted with following parameters: the on-site Coulomb energy, $U_{dd} = 5.5$ eV, the charge transfer energy from O $2p$ to Co $3d$, $\Delta = 3.5$ eV, the Slater-Koster integral for the O $2p$–Co $3d$ hybridization, $V_{pd\sigma} = -2.0$ eV, and the Coulomb attraction between the core hole and a Co $3d$ electron, $Q = 1.25U_{dd}$. With these parameter values, even when the oxygen $2p$ band width is as large as

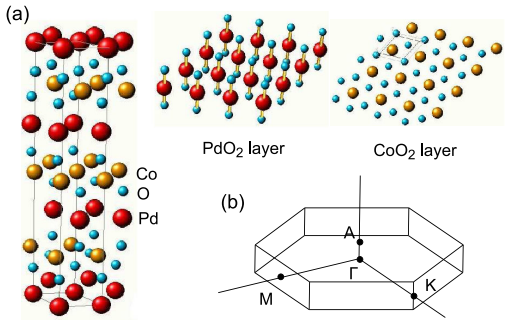

FIG. 1 (color online). (a) Crystal structure of delafossite-type $PdCoO_2$. A PdO_2 layer and a CoO_2 layer are stacked alternately along the z direction. (b) Brillouin zone of $PdCoO_2$ corresponding to the hexagonal unit cell.

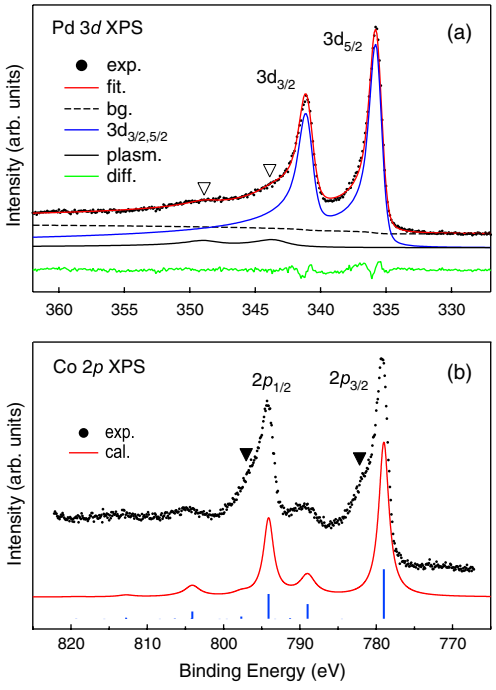

FIG. 2 (color online). (a) Pd $3d$ XPS spectrum of $PdCoO_2$ (black dots), simulated spectra based on the DS line shape model (solid lines). (b) Co $2p$ XPS spectrum of $PdCoO_2$ (black dots), calculated spectrum based on the configurational interaction cluster model (red solid line), and relative transition amplitudes of the photoemission process (blue bars).

3 eV, the CoO_2 layer belongs to a charge transfer insulator in the Zaanen-Sawatzky-Allen phase diagram [22]. The shoulder peak (▼) at the lower binding energy in each main line is attributed to a surface-related structure [23], and is not included in the model calculation. The ratio of in-plane conductivity, $\sigma_{\|}$, to the out-of-plane conductivity, $\sigma_{\perp}$, is as large as ~200 [10]. Not only the two-dimensional crystal structure but also the metal-insulator stack structure enhances the anisotropy.

More conclusive information on the electronic structure of $PdCoO_2$ is obtained from our ARPES data. Figure 3(a) shows a two-dimensional FS map, or Fermi lines, measured by ARPES. Figure 3(b) is the ARPES intensity map that shows the dispersion relation of the valence and conduction bands along the momentum region indicated by the white line in Fig. 3(a). Three bands, referred as S1, S2, and B, are clearly seen to cross the Fermi level (red dotted line), but band B differs from S1 and S2 in dispersion and character. Band B shows a sharp sp bandlike dispersion and forms an electronlike FS, while S1 and S2 show relatively weak dispersion and form holelike FS's, which are absent in the *ab initio* band calculations [11–13]. Since it is well known that ARPES is a surface-sensitive probe and that the surface electronic structure of transition-metal oxides may be quite different from the bulk one, we approached this issue both theoretically and experimentally to clarify the origin of band S1 and S2. To theoretically implement the surface states, we assume that the Pd-O bonds are broken at a cleaved surface and surface relaxation happens to reduce a surface energy. For the CoO_2-terminated surface, we performed the *ab initio* surface band calculations by using the full potential augmented plane wave method including the spin-orbit (SO) coupling. The calculated FS and band dispersions along Γ-M direction are displayed in Figs. 3(c) and 3(d), respectively, in which the calculated FS's and the dispersions of band S1 and S2 are nearly identical with the experimental ones. These two bands are the SO split Co d states. More detailed band structures related with various surface configurations will be published elsewhere. Experimentally, we increased the sample temperature to remove surface states, if any, which was successfully used in Sr_2RuO_4 and Na_xCoO_2 [24]. By monitoring residual gases, the sample was cooled down again just before the partial pressure of water increased, thus the most of the outgassed were hydrogen and carbon monoxide. Figure 3(e) is a measured FS after this treatment. The surface states are completely removed, and only a large bulk FS is clearly observed. We also tried to obtain ARPES spectra at lower photon energies (less than 50 eV) for better energy and momentum resolution, which produced the same FS's with in Fig. 3(a) for a freshly cleaved surface, but bulk band B was hardly seen probably due to small photoelectron escape depth and the contaminated surface.

An explicit connection between the high in-plane conductivity and the bulk electronic structure can be established by analyzing the ARPES data. The conductivity tensor, σ_{ij}, of a solid system is given by a solution of the Boltzmann equations [25]: $\sigma_{ij} = e^2 \int_{-\infty}^{\infty} d\varepsilon \sum_{\vec{k}}^{BZ} (-\frac{\partial f_0}{\partial \varepsilon}) \times \tau_k v_i v_j \delta(\varepsilon - \varepsilon_{\vec{k}})$, where the summation is over the first BZ, ε_k is the dispersion relation of the electrons in a solid, f_0 is the Fermi-Dirac distribution function, $v_i = \frac{1}{\hbar} \frac{\partial \varepsilon}{\partial k_i}$ ($i = x, y, z$) is the carrier velocity, and τ_k is the carrier lifetime. As the conductivity equation says, it can be calculated with the electronic structure parameters that are directly measured by ARPES. Since the photoemission process corresponds to single particle excitation, the spectral width of the excitation measures the inverse lifetime of the photohole. When the photohole lifetime is measured at the Fermi level it corresponds to the carrier lifetime. Figure 4 explains this procedure. After the surface states were removed by the thermal cycle method, the ARPES spectra were obtained along the Γ-M direction as shown in Fig. 4(a). Here, only bulk band B is seen in the image. The energy distribution curves (EDC) at momentum ranging from $k_{\|} = 0.6$ to 1.2 $Å^{-1}$ are displayed in Fig. 4(b). A sharp dispersion of band B is observed in these plots. The carrier velocity is measured to be 4.96(3) eV Å/$\hbar$ from this dispersion. The

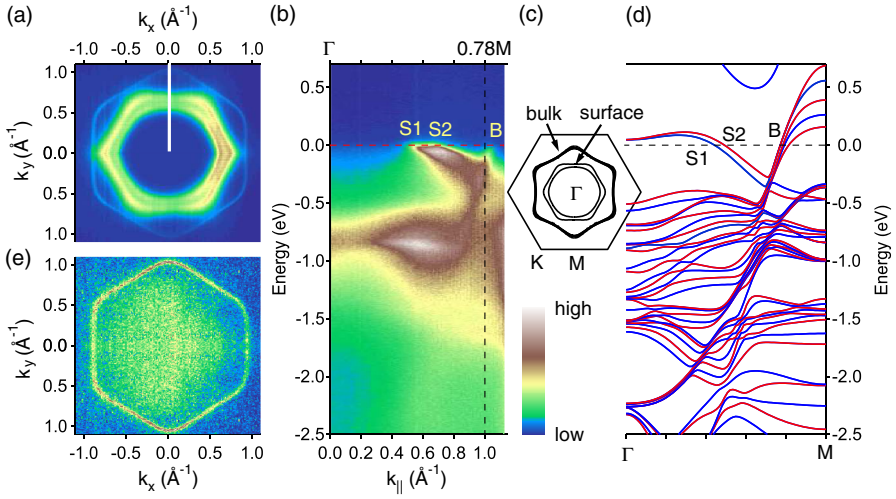

FIG. 3 (color online). (a) Constant energy ARPES image obtained from a fresh cleavage surface of $PdCoO_2$ at the Fermi level. (b) ARPES intensity map along the Γ-M direction. The intensity of the images is drawn in the terrain color scale as shown in the scale bar at the right side. (c) Brillouin zone (hexagon) and bulk and surface FS's by the *ab initio* band calculation. (d) Calculated band dispersions along the Γ-M direction. The SO coupling and lattice relaxation effect at the CoO_2-terminated surface are taken into account in the calculation. (e) Constant energy ARPES image obtained after removing the surface states.

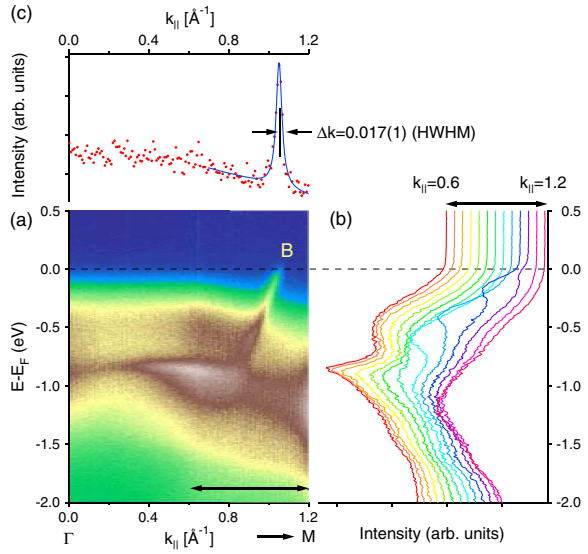

FIG. 4 (color online). (a) ARPES intensity map of $PdCoO_2$ along the Γ-M direction with the surface states removed. The intensity scale is the same as in Fig. 3. (b) Energy distribution curves at momentum ranging from $k_{\|} = 0.6$ to 1.2 Å^{-1}. (c) Momentum distribution curve at the Fermi level.

momentum distribution curve (MDC) at the Fermi level is shown in Fig. 4(c). The peak width in half width at half maximum (HWHM), $\Delta k = 0.017(1)$ Å^{-1}, in the MDC corresponds to the inverse mean free path, $1/l_{\mathrm{MFP}}$. Thus, the carrier lifetime is given by $\tau = l_{\mathrm{MFP}}/v_k = 1/v_k\Delta k = 7.6(4) \times 10^{-15}$ s. Now we assume that the in-plane conductivity is isotropic within the ab plane and that the carrier lifetime is independent of the momentum for simplicity, then the integration of $\tau v_x v_x$ over the first BZ and near the Fermi energy gives the in-plane conductivity. The real calculation can be approximately done by section-wise summation over the ARPES-measured FS under neglecting the variation of FS along the k_z direction, resulting in $\sigma_{\|} = 7.5(2) \times 10^4$ $(\Omega\mathrm{cm})^{-1}$. Inversely, the calculated resistivity from the ARPES data is $\rho_{\|} = 13(1)$ $\mu\Omega$cm. This gives a reasonable agreement with the transport measurement results [7,10] when we consider that the measured inverse lifetime is broadened by surface conditions and an instrumental resolution. Judging from the fact that the ARPES-measured conductivity and the conventional dc conductivity at room temperature are of the same order of magnitude, the peak width in Fig. 4(c) is resolution limited, and a higher angular resolution is required in order to explain even the temperature dependence of the conductivity. A close inspection of the procedure for the conductivity calculation reveals the reason why the system has the low resistivity: (i) The band crossing the Fermi level has a sharp sp-like dispersion which gives a high carrier velocity in the system. (ii) The carrier lifetime is as long as that of a simple metal. (iii) The system has a large two-dimensional FS. These three factors make the resistivity of the oxide remarkably low.

In summary, we have presented the Pd $3d$ and Co $2p$ core-level XPS spectra and the ARPES spectra of delafossite $PdCoO_2$. The contrasting feature of the XPS spectra supports that the system can be regarded as a metal-insulator stack structure and explains why the system has large anisotropy in the electric conductivity. The analysis of the ARPES spectra, which establishes an explicit connection between the conductivity and the electronic structure, reveals that the high conductivity of the system originates from the sharp dispersion of the conduction band, the large two-dimensional FS, and the long lifetime of the carriers.

This work was supported by the KOSEF grant funded by the Korea government (MEST) (No. R01-2008-000-10666-0). This work was also supported by the KRF grant funded by the Korean government (MOEHRD, Basic Research Promotion Fund, KRF-2008-314-C00086). B. I. M acknowledges the support of the KOSEF through the eSSC-POSTECH.

*ffnhj@chonnam.ac.kr
†hdkim@postech.ac.kr

[1] P. W. Anderson, Science **235**, 1196 (1987).
[2] J. A. Wilson *et al.*, Adv. Phys. **24**, 117 (1975).
[3] S. Y. Zhou *et al.*, Nature Phys. **2**, 595 (2006).
[4] R. D. Shannon *et al.*, Inorg. Chem. **10**, 713 (1971).
[5] H. Kawazoe *et al.*, Nature (London) **389**, 939 (1997).
[6] T. Otabe *et al.*, Appl. Phys. Lett. **72**, 1036 (1998); M. S. Lee *et al.*, Appl. Phys. Lett. **79**, 2028 (2001).
[7] M. Tanaka *et al.*, J. Phys. Soc. Jpn. **65**, 3973 (1996).
[8] David R. Lide, *CRC Handbook of Chemistry and Physics*, Section 12, Properties of Solids (CRC Press, Boca Raton, FL, 2003), 84th ed.
[9] M. Tanaka *et al.*, Physica (Amsterdam) **245B**, 157 (1998).
[10] H. Takatsu *et al.*, J. Phys. Soc. Jpn. **76**, 104701 (2007).
[11] R. Seshadri *et al.*, Chem. Mater. **10**, 2189 (1998).
[12] H. Okabe *et al.*, J. Appl. Phys. **93**, 7258 (2003).
[13] V. Eyert *et al.*, Chem. Mater. **20**, 2370 (2008).
[14] H.-D. Kim *et al.*, AIP Conf. Proc. **879**, 477 (2007).
[15] G. D. Mahan, Phys. Rev. **163**, 612 (1967).
[16] P. Nozières and C. T. De Dominicis, Phys. Rev. **178**, 1097 (1969).
[17] S. Doniach and M. Šunjić, J. Phys. C **3**, 285 (1970).
[18] S. Hüfner and G. K. Wertheim, Phys. Rev. B **11**, 678 (1975).
[19] G. K. Wertheim and S. Hüfner, Phys. Rev. Lett. **35**, 53 (1975).
[20] J. Park *et al.*, Phys. Rev. B **37**, 10 867 (1988).
[21] A. E. Bocquet *et al.*, Phys. Rev. B **46**, 3771 (1992).
[22] J. Zaanen *et al.*, Phys. Rev. Lett. **55**, 418 (1985).
[23] This was confirmed by that the shoulder peak intensity increases relative to the main and satellite peaks after a thermal-cycling (20–120 K) treatment to remove the surface states in the valence bands ARPES spectra.
[24] A. Damascelli *et al.*, Phys. Rev. Lett. **85**, 5194 (2000); H.-B. Yang *et al.*, Phys. Rev. Lett. **95**, 146401 (2005).
[25] G. D. Mahan and J. O. Sofo, Proc. Natl. Acad. Sci. U.S.A. **93**, 7436 (1996).